

Development of a Bridge Weigh-in-Motion Sensor: performance comparison using fibre optic and electric resistance strain sensor systems

Myra Lydon, S E Taylor, Desmond Robinson, Paul Callender, Ciaran Doherty, S K T Grattan and Eugene J OBrien

Abstract—This research addresses the problems of effective *in situ* measurement of the real time strain for bridge weigh in motion (B-WIM) in reinforced concrete bridge structures through the use of optical fibre sensor systems. By undertaking a series of tests, coupled with dynamic loading, the performance of Fibre Bragg Grating-based sensor systems with various amplification techniques were investigated. In recent years, Structural Health Monitoring (SHM) systems have been developed to monitor bridge deterioration, to assess load levels and hence extend bridge life and safety. Conventional SHM systems, based on measuring strain, can be used to improve knowledge of the bridge's capacity to resist loads but generally give no information on the causes of any increase in stresses. Therefore, it is necessary to find accurate sensors capable of capturing peak strains under dynamic load and suitable methods for attaching these strain sensors to existing and new bridge structures. Additionally, it is important to ensure accurate strain transfer between concrete and steel, the adhesives layer and the strain sensor. The results show the benefits in the use of optical fibre networks under these circumstances and their ability to deliver data when conventional sensors cannot capture accurate strains and/or peak strains.

Index Terms—Fibre optic sensors, Structural Health Monitoring (SHM), strain measurement

I. INTRODUCTION

Much of the bridge stock on major transport links in North America and Europe was constructed in the 1950's and 1960's and has since deteriorated or is carrying loads far in excess of the original design loads. Bridge "Health Monitoring" systems have been developed to monitor bridge deterioration and hence bridge safety but these systems are only telling half the story. Conventional bridge health monitoring systems can improve knowledge of the bridge capacity but give no information on the causes of increased stresses. The mass of freight carried is growing rapidly – In Europe it has been estimated that the tonne-km has increased by over 30% in the past ten years. The situation in the US is very similar. To monitor bridge safety, we need to have information on the frequencies and weights of heavy trucks as well as on the bridge condition. Among our infrastructure, a significant portion of bridges are classified as insufficient for purpose. The situation is expected to become worse because of the proportion of infrastructure that is showing problems. The solution to the bridge safety problem is twofold: control of overloaded trucks and safety assessment/monitoring of bridges. Weigh-in-Motion (WIM) techniques have been traditionally used for measuring vehicles' weights while travelling at highway speed. WIM systems provide detailed data on gross vehicle weights (GVW), individual axle loads, velocities and axle spacing of almost all vehicles passing the system. However, as they are placed in the road pavement they are subject to pavement wear and or replacement. Additionally, the accuracy is limited – typically 95% of gross weights are within $\pm 7\%$ in the better installations and axle weight accuracy is worse. WIM systems are calibrated to typical highway speeds and become less accurate at lower speeds and the calibration curve tends to shift with temperature change, decreasing the accuracy if not continually recalibrated[1]. Bridge WIM (or B-WIM) is a special type of WIM that uses a sensor network at the bridge soffit to determine passing axle weights at any speed. In the late 1970's Moses [2] developed a B-WIM algorithm using the strain history to estimate the axle weights of the passing vehicle. The measurements were recorded for the entire duration of the vehicle's passing over the structure. This is advantageous, compared with pavement WIM where measurement of an axle lasts only a few milliseconds. The algorithm to process the data is based on the assumption that when a moving load is applied to a bridge this will cause the longitudinal members to bend in proportion to the product of the magnitude and the influence line. The next significant step in B-WIM development was as a result of a series of projects funded by the European Commission such as COST 323 [3] and subsequently The Weigh in motion of Axles and Vehicles for Europe (WAVE) project[4]. The main work addressed improvements of accuracy, user-friendliness, portability and durability of these systems. The commercial B-WIM system SiWIM was developed from the WAVE project. More recent field studies have found that the results obtained are more accurate when the influence line is calculated from direct measurements rather than theoretical predictions[5]

In order to achieve successful B-WIM, a very high scanning rate and sub microstrain accuracy (or amplification) of the sensors, is required to capture the peak strains induced in the bridge structure by the moving vehicles. Additionally, the sensors can measure the velocity and axle configuration of any vehicle by applying a suitable algorithm to the measurements during post

processing[6]. This system has the potential to provide an inexpensive portable method of rapidly retrieving unbiased traffic surveys. The deployment of such a system would be desirable as it would enable the collection of data for planning and economic surveys and would be of great benefit to the network asset owners [7]. This research explores beyond the current state of the art technology to recommend concepts and potential additional sensor technology which would overcome the existing limitations of the current technology. Expanded use of alternative sensor technology will be considered coupled with the concepts for solution algorithms, data pattern recognition and information processing. Additionally, this new generation B-WIM is intended to fully replace WIM and pick up all axle loads including cars so data on traffic and speeds can also be gathered for the Roads Service / PSNI. The full FEA of this bridge showed that the largest strain was 30 microstrain for an overloaded 6 axle truck, less than 5 microstrain for a light goods vehicle and about 1 microstrain for a car on the slab. All of these values decrease when the wheel is above the beam/girder – hence the need for amplification is the main driver in these laboratory trials.

The research work reported in this paper presents an innovative approach to amplify the strain signal using fibre optic strain (FOS) sensors which have been developed using Fibre Bragg Grating (FBG) technology. Their performance was examined and compared with the performance of more conventional electrical resistance strain (ERS) sensors and vibrating wire (VW) strain sensors. The overall aim of this research programme is to detect strains and related changes in the bridge structure caused by an axle moving at highway speed. This experimental study investigated strain transfer mechanisms and amplification techniques. The bridge structure in this study is a typical medium span reinforced concrete bridge. A finite element analysis of the structure predicted very low levels of change in strain under typical axle load and the B-WIM algorithms require a distinct change in strain to accurately determine axle weights. Therefore amplification was required to improve the accuracy below sub microstrain. Additionally, an accurate sensor network with the capability of high scanning rates, can provide an ‘early warning’ of damage and allow for the planning and implementation of remedial action to the structure at a point where it is less expensive and invasive than when visible surface signs of deterioration have been observed. In this paper, tests were carried out to provide comparative data between conventional ERS sensors and fibre optic sensors and to enable a comparison of performance under controlled conditions representing fixing to a bridge deck slab. Additionally, an amplification technique for improving sub-microstrain accuracy has been developed and is now being used in a real bridge deck in the UK for B-WIM. Conclusions on the suitability of the fibre optic sensors (FOS) for long-term structural health monitoring of reinforced concrete bridge structures have been made.

II. SENSOR SYSTEMS FOR B-WIM

A. Fibre Bragg Grating sensors

The FOS used in the research was based on Fibre Bragg Grating (FBG) technology. Tensile and compressive strains, measured at a bridge soffit can be used as a means of detecting axle position, configuration and weights using suitable post-processing as described earlier. To measure the tensile and compressive strains, FBG sensors can be adapted from other industrial monitoring applications[8]. Previous work on the use of Fibre Bragg Grating sensors for strain measurement has been extensively documented in the literature, e.g. [9], [10]and such sensors have been developed for measuring rapid, dynamic changes and long-term performance of concrete bridges and composite steel-concrete box structures [11]–[13]but this packaged FBG technology has not been used for sub microstrain measurements needed for accurate Bridge Weigh-in Motion under dynamic moving loads.

Fibre Bragg Gratings (FBGs) for tensile and compressive strain measurements rely upon the induced strain in the sensor causing a change in the characteristic wavelength of light reflected back along the optical fibre. The equation used to determine the central reflected wavelength, λ_B , is defined by the Bragg condition given in Equation 1:

$$\lambda_B = 2n_e\Lambda \quad (1)$$

where n_e is the effective refractive index of the fibre core and Λ the periodic spacing of the grating [8]. The increase in applied strain can be calibrated against the shift in wavelength (λ) observed across the FBG whose periodic spacing (Λ) has increased. The value of λ_B used is in the region around ~ 1550 nm. FBGs are written into Boron-Germanium doped optical fibre which is recoated to restore the original mechanical strength of the fibre [14], [15]For FBG-based B-WIM sensors for monitoring the localised strain several different packaging and amplifying systems together with fixing techniques were investigated. The optical sensors can be multiplexed along very long lengths of fibre, are well suited to large structures and can be set accurately by placing the FBGs at pre-determined points along a configured optical sensor network. The two-fold nature of the sensor system is designed to ensure (i) a greater region (length) of coverage by the monitoring system whilst (ii) allowing a greater number of B-WIM sensors to be placed in the areas predicted to be most sensitive. In the case of B-WIM, these positions are based on peak stress areas established using finite element analysis (FEA).

The sensors can be surface mounted to existing structures or embedded in the structure during the construction phase and the discrete nature of the sensors equates to less interference in structural behaviour compared with larger embedded sensors, such as VW. FBG’s have potential for application across various industries, in the civil industry the focus is primarily on strain and temperature measurement. As FBG’s respond to both temperature induced strain and mechanically induced strain, it is important to remove the thermal output from the strain in order to determine the true mechanically induced strain. Temperature can either

internally compensated in the sensor or done via a separate temperature sensor. For internal compensation the following formula is used:

$$\varepsilon = (10^6 \mu m/m) \left[\left[\frac{\Delta WL/WL_0}{F_G} \right]_{Strain} - \left[\frac{\Delta WL/WL_0}{C_1} \right]_{Temp} \right] - (CTE_S - C_2) \frac{(10^3 pm/nm) \Delta WL_{Temp}}{S_T} \quad (2)$$

ε = Stress induced Strain

ΔWL_{Strain} = Wavelength Shift [Strain Grating](nm)

$WL_{0Strain}$ = Initial Reference Wavelength [Strain Grating] (nm)

ΔWL_{Temp} = Wavelength Shift [Temp Grating](nm)

WL_{0Temp} = Initial Reference Wavelength [Temp Grating] (nm)

CTE_S = Coefficient of Thermal Expansion-Substrate ($\mu m/m-^{\circ}C$)

C_1 = Sensor Constant 1 [Gage factor Temp.Grating]

C_2 = Sensor Constant 2 [Specified Sensor CTE] ($\mu m/m-^{\circ}C$)

S_T = Temperature Sensitivity [Temp Grating] ((pm)/($^{\circ}C$))

Three types of FBG's sensors were compared, focusing on site suitability, fixing methods and accuracy. FBG1 was a non-metallic strain sensor based on FBG technology which could be quickly and easily mounted in place using a specialized two component low viscosity modified amine epoxy. The epoxy develops 90% of its cure properties at 24 hours, the full cure time is 72 hours. When fully cured the epoxy inherits a tensile strength of 31N/mm², tensile modulus of 6,700 N/mm² and a compressive strength of 80 N/mm². The sensor has a self-adhesive backing which holds it in place while the epoxy is injected and encapsulates the fibre thus fixing the sensor; this sensor has a gauge length of 10mm and a packaged sensor length of 20mm. Temperature compensation is carried out using an additional temperature sensor which is attached to the structure. One temperature sensor can be used for temperature compensation of numerous strain sensors. FBG2 had a 50mm gauge length; it is a temperature compensated strain sensor based on FBG technology and has a packaged sensor length of 136mm. A more accurate long-term strain measurement can be provided due to the close proximity of the individual strain and temperature FBGs in one sensor. The sensors rugged design makes it suitable for long term monitoring in harsh weather conditions, [16] and armoured cables lead from the sensors protecting the fibre cable. FBG3 has a gauge length of 250mm and a packaged sensor length of 300mm; it is surface mounted sensor based on FBG technology and is also internally temperature compensated. Each end of the sensor is attached to the structure via rigid brackets that are welded, doveled, epoxied, or grouted to the surface of a material or structure.

B. ERS Sensors

Electrical resistance strain sensors with gauge lengths of 5mm (ERS1) and 30mm (ERS2) were trialled; the surface was prepared as recommended [17]. As the material is strained the foil is deformed causing the electrical resistance to change, which is calibrated to the equivalent change in strain by the gage factor (GF):

$$\varepsilon = (\Delta R/R_G)/GF \quad (3)$$

ε = Strain, ΔR = Change in resistance, R_G = Resistance of the undeformed sensor

C. VW Sensors

Vibrating Wire sensors are surface mounted; a change in strain on the surface causes a change in tension in the wire which results in a change in the resonant frequency of oscillation of the wire. This change is calibrated to the equivalent change in strain between the fixings. If the VW is perpendicular to a crack in concrete it can be assumed that all of the strain change is caused by the cracking opening and the VW sensor is thus measuring crack width. In this test a 100mm sensor was used.

D. Data collection and logging

Data from the FBG, VW and ERS sensors were obtained and recorded during the progress of the series of experiments carried out and described below. Data acquisition was carried out using commercially available software and interrogation units for each of the sensor types. The scanning rate capability of the sensors is a critical factor in selecting an appropriate sensors, the data from the Phase 1 tests, as detailed below (IV) was recorded at different scanning rates. The scanning rate was limited to the maximum scanning rate of the slowest sensor included in the test. Hence, the scanning rate of each sensor included in an individual test was all set the same allowing ease of comparison when considering the results.

Each testing Phase included only short term tests therefore the data from all sensors was continually monitored during the full test process. The ERS sensors record a direct change in strain, the VW sensor acquisition unit logged a change in frequency which was subsequently converted to a change in strain. Similarly, the wavelength shift data associated with the FBG-based sensor was recorded; this was done using a combined light source and interrogation unit, in conjunction with post-processing software to convert the change in wavelengths to equivalent change in strain.

Additionally load was recorded directly from the direct tension testing machine with its accompanying software. This ensured

effective comparisons between the performance of the fibre optic sensor and conventional strain sensors.

III. EXPERIMENTAL PROGRAMME

The aim of the work was to conduct a series of sequential tests in which a number of different fixing techniques, with representative conditions of a concrete bridge deck soffit (underside of the bridge), were evaluated. The bridge structure selected for this B-WIM research consisted of 27 no. pre-stressed precast concrete Y4 beams and a cast in-situ concrete deck. The bridge spans 19 m and has an angle of skew of 22.7°. Accurate B-WIM requires sensors to be attached to the longitudinal members and deck soffit of the bridge structure. The beam sensors can be fixed directly to the soffit of the concrete beams. However, the bridge deck had been cast using permanent Glass Fibre Reinforced concrete (GFRC) formwork. A site survey revealed the formwork could not be removed without damage to the structural concrete deck slab. Hence, the proposed method of fixing involved attaching the sensors to a stainless steel plate which could then be fixed to the structural element. The testing phases detailed were carried out in order to determine a suitable sensor, plate geometry for amplification and fixing method.

IV. PHASE 1: PERFORMANCE COMPARISON OF SENSORS FOR B-WIM

A. Testing Procedure

The initial testing was aimed at providing a performance comparison between two types of FBG's, VW and ERS1 sensors and inform on the type of sensor which was most suitable for SHM for B-WIM applications. All four sensors were fixed onto a 200×100mm stainless steel plate as shown in Fig. 1. The surface was cleaned thoroughly and neutralised prior to attaching the different strain sensors, this was done to ensure a good bond for the attachment of the ERS but this was not necessary for the FBG-based sensors. After all of the sensors had been attached and recommended curing time for each of the adhesives had elapsed the plate was then tested. The test was carried out using a direct tension testing machine with a load capacity of 100kN. Load was applied, under stroke control, at a rate of 0.01mm/min. The highest scanning rate for the data acquisition of the VW was 0.2Hz for accurate strain readings. Therefore, for comparison purposes, the scanning rate for all sensors was set the same at 0.2Hz. The length of the temperature compensated FOS was incompatible with the maximum settings of the test rig cross-heads and affected plate clamping which resulted in some slip at an applied load of ~80N. The loading rate was increased to 1mm/min which was sufficient to ensure full clamping of the plate and then only limited slip occurred during loading. Data acquisition/FOS interrogation was carried out using three separate systems, to enable comparison of the results for the different sensors, the time stamps for each system were synchronised. The details of the FBG sensors were as follows:

FBG 1 – initial wavelength 1541.68nm – glued

FBG 2 – initial wavelength 1523.81nm – glued

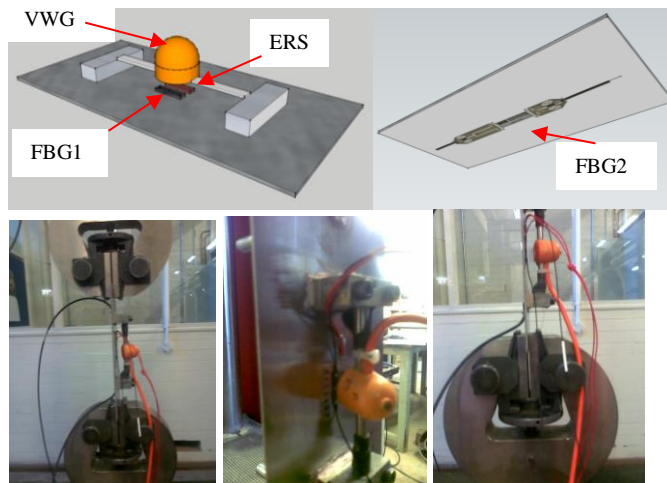


Fig. 1. Phase 1: Sensor arrangement and set up configuration for test.

B. Results and Discussion

For accurate B-WIM predictions, a minimum scanning rate of 200Hz is required but more typically about 500Hz. In these tests, VW, FBG and ERS sensors were tested in direct tension on a steel plate at various scanning rates. The results in Fig. 2 show that the sensors gave reasonably accurate predictions of the tensile strain – when the strain between the cross-heads (equivalent to the strain in a concrete deck), or ‘test-rig’ strain was $42\mu\epsilon$, the strains in FBG1, FBG2, VW and ERS1 were $59\mu\epsilon$, $25\mu\epsilon$, $66\mu\epsilon$ and $61\mu\epsilon$ respectively. However, the results indicate that bending occurred in the plate which increased the tensile strain on one face and decreased the tensile strain on the other face. The VW debonded at a strain value of $75\mu\epsilon$, this coupled with a maximum accurate scanning rate 0.2Hz for the VW data acquisition deems this type of sensor unsuitable for dynamic strain measurement and B-WIM applications.

The axial tensile strain can be determined from the average of FBG1 and FBG2 which will remove the strain due to bending. This showed that the FBG gave slightly better correlation to the data acquisition from the tension testing machine which has an accuracy of $\pm 1\mu\text{e}$ – at a ‘test-rig’ strain of $71\mu\text{e}$, the strain averaged from FBG1 and FBG2 was $73\mu\text{e}$ compared with the average strain from ERS1 and FBG2 which was $74\mu\text{e}$ as shown in Fig.3.

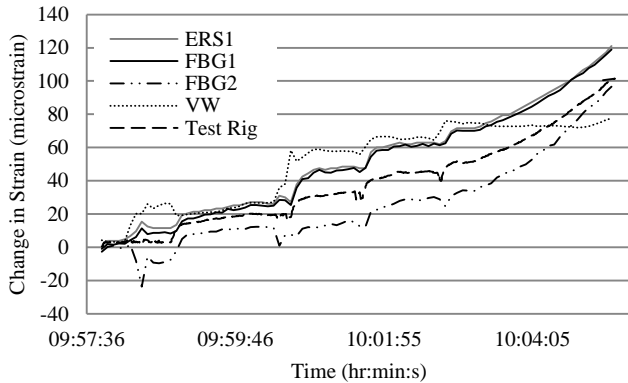


Fig. 2. Phase 1: Strain vs. time results at 0.2Hz scanning rate for three types of sensor

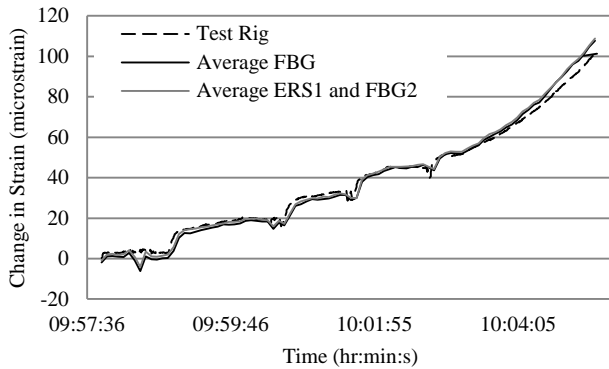


Fig. 3. Phase 1: Axial Strain vs. time results at 0.2Hz scanning rate for two types of sensor

However, in order to further compare the accuracy of the ERS and FBG’s, the test was repeated without the VW and the sensors interrogated at a higher scanning of 5Hz. Good accuracy was achieved in both types of sensor and correlated well with the strain data from the test machine. However when the results were averaged to present only the axial strain, the FBG provided better accuracy, at a ‘test-rig’ strain of $64\mu\text{e}$, the strain averaged from FBG1 and FBG2 was $64\mu\text{e}$ compared with the average strain from ERS1 and FBG2 which was $60\mu\text{e}$ as shown in Fig. 4.

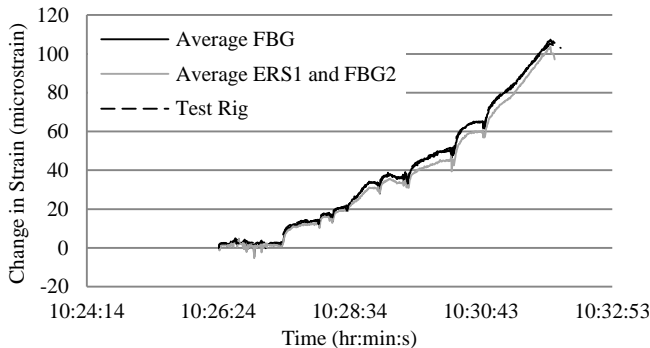


Fig. 4. Phase 1: Axial Strain vs. time results at 5Hz scanning rate for two types of sensor

The main issue that is faced with the ERS sensors is that of the temperature effects: both the gauge and that which is being measured can be affected by this. As a result, self-compensating gauges have been produced, which have been shown to have little apparent alteration in changing temperature conditions. These sensors however have a very narrow range of application in terms of temperature and specimen material[18]. In the case of FBG sensors temperature compensation can be easily carried out through strain isolation of the FBG, as demonstrated in Eq 2. There are many other advantages in using FBG sensors; they demonstrate a linearity in response over many orders of magnitude, and they are flexible and have a higher temperature tolerance. The packaged sensors used in this trial have a greater ease in fixing, there is not the same need for surface preparation

and thereby the skill of the person installing them has less of an impact on the potential accuracy of the results obtained.

FOS can be multiplexed, this means the possibility of hundreds of sensors along the length of a single fibre. The equivalent for ERS would be then 100s of wires being run back to a single interrogation point, which can lead to potential complications and confusion, again for an inexperienced user. Should an issue arise with the hardware interrogating the equipment for FOS this can be easily replaced with minimal setup, once the configuration file is developed the interrogating unit can be replaced in seconds which is not the case for ERS.

The environmental conditions on site also needed to be considered when choosing an appropriate sensor, the damp weather conditions in the UK and Ireland require a durable sensor, ERS have the potential to corrode, as they are metallic, this is not an issue for FOS which are silica based. ERS have the advantage of being easily repaired if they are fractured on site, however with the increasing technology in portable splicers this is becoming less of an issue for FOS. FOS also allow for connectors to be added between each sensor so if one sensor in a series is damaged it can easily be replaced. Multiplexing options for FOS include wavelength multiplexing, time division multiplexing (TDM), frequency division multiplexing (FDM) etc, which are tried and tested and allow for this use of multiple sensors per fibre FOS have been used in real-life conditions over multiple kilometres of fibre,

FOS are EMI immune, which in today's world is a very important aspect to be had, without having equipment to measure the levels, then you are operating with that risk with the ERS which you are not with FOS, this is an advantage for particularly in railway bridges where the train passing can interfere with ERS gauges.

A further issue encountered in relation to the ERS sensors was the difficulty in fixing the sensor to the surface compared with the ease of fixing the packaged non-metallic optical sensor. The surface preparation, electrical insulation with the fixing of this ERS sensor was far more labour intensive. In order to install the B-WIM System on site road closures were required these closures were costly and disruptive and it was vital that the chosen system could be easily and quickly installed so as to provide minimum disruption to the road network. Therefore, ERS sensors with the current data acquisition were not deemed suitable for the practical development of a full B-WIM system. However, the results show ERS provide accurate results and therefore they were used for subsequent tests for comparing fixing methods for the plate and for the development of a plate for geometry for maximum strain amplification. The use of FBG's for all tests would have substantially increased to cost of the project and as the tests were carried out in a controlled environment and the sensors were not to be exposed to harsh weather conditions durability was not an issue. As well as this the time allowed for accurately fixing the sensors was not governed by road closures and multiplexing would be of little benefit as only a small number of sensors were required.,

From the tests in Phase 1 it was determined that FBG1 was the most suitable as it was easily mounted and quick to adhere to both steel and concrete surfaces. FBG2 has a higher gauge length and an overall packaged length of 136mm which made it impractical for fixing directly at the concrete slab soffit. Additionally, to enable amplification, the plate would be much larger and could lead to lower accuracy in detecting the absolute peak strain under a moving axle load as the strain would increase over a longer period of time.

V. PHASE 2: FBG/ERS SENSORS WITH MODIFIED PLATE GEOMETRY FOR STRAIN AMPLIFICATION

A. Testing Procedure

It had already been determined that a fixing plate was required in order to measure the change in strain in the concrete bridge deck under live traffic loading. The critical sensor locations were established using finite element analysis (FEA) of a full 3D model of the bridge. The results from the FEA indicate the change in strain in the bridge deck would be low even under heavy loading. The largest change in strain was 30 microstrain and less than 5 microstrain for most typical traffic loading. In order to amplify the strain at the sensor location on the plate, the area in the central region of the plate was reduced. Assuming that the change in strain in the plate is consistent, the section with the reduced area gives a higher stress and hence amplified changes in strain under a set change in load (or axle load). The following theory was used to select a suitable geometry for the plate. Considering:

$$\varepsilon = \sigma/E \quad \text{and} \quad \sigma = F/A \quad \text{then} \quad \varepsilon = F/EA \quad (4)$$

where E= young's modulus, σ = Stress, A= cross sectional area, a reduction in cross sectional area results in an inversely proportional increase in strain. Consider the plate shown in Fig. 5, the plate geometry was such that the cross sectional area of the central region was one third of that of the outer regions. Therefore the change in strain in the centre of the plate would be three times that of the change in strain in the outer edges of the plate (ε_1). The following theory was then applied to establish the relationship between the changes in strain in the plate compared to the actual change in strain (ε_T) in the structural element (in this research the concrete bridge):

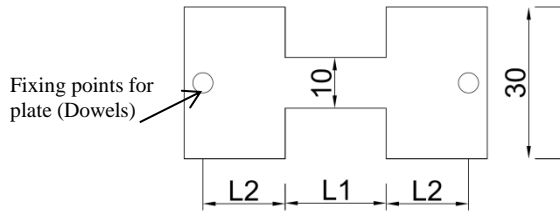


Fig. 5. Geometry of plate proposed for amplification. all dimensions in mm

Strain:

$$\varepsilon = \Delta L / L \text{ so } \Delta L = \varepsilon L, \quad (5)$$

Actual change in strain in the concrete:

$$\Delta L = \varepsilon_T (2L_2 + L_1) \quad (6)$$

Now consider the change in strain in each individual area of the plate, from (4) we know the change in strain is inversely proportional to the cross sectional area, therefore if the strain in the outer regions is ε_1 the strain in the central region is $3\varepsilon_1$:

$$\Delta L = (L_2\varepsilon_1 + L_13\varepsilon_1 + L_2\varepsilon_1) \text{ so } \Delta L = (2L_2 + 3L_1)\varepsilon_1 \quad (7)$$

Amplification factor:

$$\text{Equating (6) \& (7) } \varepsilon_1 = \frac{\varepsilon_T(2L_2+L_1)}{(2L_2+3L_1)} \quad (8)$$

where L_1 and L_2 are the lengths as shown in Fig. 2 and ΔL = change in length.

Based on this theory, a spread sheet was used to calculate the optimum geometry of the plate in order to amplify the change in strain by a factor of three. The dimensions of the plate used for testing are 70mm, 35mm, and 100mm consecutively for L_1 , L_2 and the width, stainless steel dowels were used to replicate the fixing to the concrete surface. Three sensors were attached using the same fixing technique as described in section II. The three sensors were two ERS1 sensors, one attached each side of the plate to take account of bending strain and FBG1 attached to one side of the plate. The plate and sensors were tested in a similar manner to Test 1 but with a stroke control rate of 1mm/min and a scanning rate of 5Hz for all sensors. The scanning rate was limited by the data acquisition for the ERS sensors as the FBG sensors can be interrogated at 2000Hz.

B. Results and Discussion

As discussed, the geometry of the plate was adjusted in order to amplify the strain in the central region of the plate compared to that in the concrete bridge deck. FBG and ERS sensors were used and strains were recorded in a similar way to Phase 1 with a scanning rate of 5Hz. The results, as shown in Fig. 6, indicate strain amplification was not successful. When the strain between the cross-heads (equivalent to the strain in a concrete deck), or 'test-rig' strain was $87 \mu\varepsilon$, the strains in FBG1, ERS1 and ERS2 were $104 \mu\varepsilon$, $74 \mu\varepsilon$ and $67 \mu\varepsilon$ respectively. Additionally, when taking into account the bending in the plate, ERS1 appears to be inaccurate and corroborates the findings in Phase 1. An FEA of the test configuration was carried out and it showed that a stress concentration occurred at the corners of the plate due to the sharp change in cross-section. Hence, the plate geometry was adjusted to give a smoother transition when reducing cross sectional area.

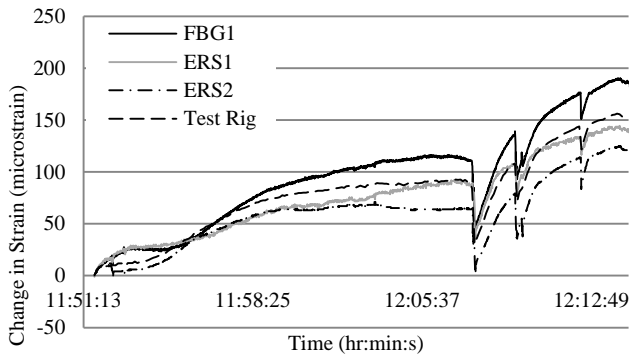


Fig. 6. Phase 2: Axial Strain vs. Time at 5Hz scanning rate.

VI. PHASE 3: ERS SENSORS WITH FURTHER MODIFIED PLATE GEOMETRY AND FIXED TO EQUIVALENT CONCRETE BRIDGE SECTION

A. Testing Procedure

Following the results of Phase 2 the geometry of the plate was modified to reduce the effect of stress concentration. This test was also carried out to determine a suitable method of fixing the steel plate to a concrete structure. The plate was mounted to a concrete section which represented a real concrete bridge. Hence, allowing a comparison to be made between the actual strain in the concrete and the amplified strain in the central region of the plate. This test used ERS sensors as it is more cost effective in testing the fixing method as a high scanning rate was not required. The geometry of the plate is shown in Fig. 4 was fabricated using 2mm thick stainless steel and the stainless steel dowels were welded in place as shown in Fig. 7. ERS1 sensors were attached to both sides of the plate and one ERS2 sensor was attached to the surface of a 3.5m long by 200mm deep by 120mm wide reinforced concrete beam directly below the plate (see Fig. 7).

A smooth non porous surface is required to enable effective bond between the concrete surface and the strain sensors and to ensure accurate strain transfer. The concrete surface, where the sensor was located, was prepared by smoothing the surface using manual sanding and filling any potential micro gaps with a layer of specialist two-component room-temperature-curing polyester adhesive. After 24 hours curing, this was smoothed using light manual sanding and the sensor was then bonded to prepared surface using an ethyl cyanoacrylate based commercial adhesive.

The plate was fixed to the bottom surface of the concrete beam at the midspan, the position of maximum bending moment. A two-part thixotropic epoxy adhesive was used to fix the 10mm diameter dowels which were embedded in 12mm diameter holes to allow for a 1mm adhesive line around the dowels. The plate was positioned 5mm from the surface of the concrete giving 40mm embedment length (Fig. 7). The epoxy was left for 3 days to fully cure.

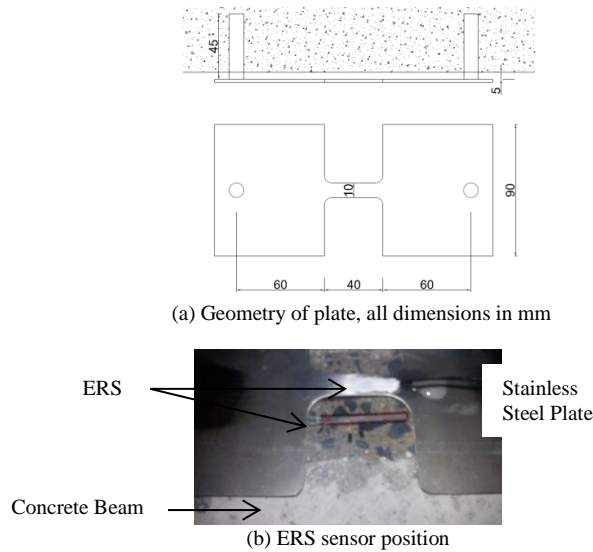


Fig. 7. Phase 3: testing layout

The concrete beam was simply supported under the test rig and load was applied at the third spans to enable pure flexure in the central region of the beam. Load was applied incrementally using an accurately calibrated 600kN capacity hydraulic actuator. Load was applied in 1kN increments under load control with strain readings recorded at each increment of load. A maximum load of 8kN was applied to the beam. The test was repeated three times.

A 3D FEA of the test arrangement was carried out to predict the behaviour of the elements in the test arrangement. In order to save on computational time the planes of symmetry in the elements are exploited and only one quarter of the actual structure is modelled.

B. Results and Discussion

The geometry of the plate was further adjusted to enable amplification of strain in the central region of the plate and the plate was mounted to an equivalent concrete bridge surface. The results in Fig. 8 show that the plate did not provide the expected amplification. For example, at an applied load of 8kN, the change in strain measured at the tension face of the concrete beam was $121\mu\epsilon$ and change in strain measured in the plate, was $156\mu\epsilon$, hence providing an amplification factor of 1.29.

The results from the FEA corroborate the actual test results, at an applied FEA load of 8kN the predicted change in strain in the plate was $184\mu\epsilon$ and the predicted change in strain in the concrete was $144\mu\epsilon$ equating to an amplification factor of 1.28 (Fig 9). For B-WIM applications, a factor of at least 2 was desirable. A plot of the strain distribution in the stainless steel plate after loading, predicted that the full geometry of the plate was not utilised and behaved in contrast to the initial predicted amplification factor outlined in Section V: Equations 4 to 8

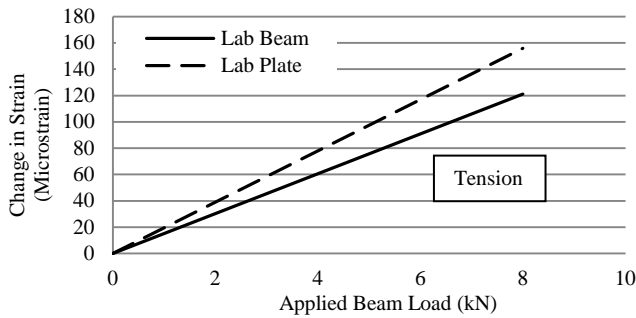


Fig. 8. Phase 3: Change in Strain vs. Applied Load (laboratory)

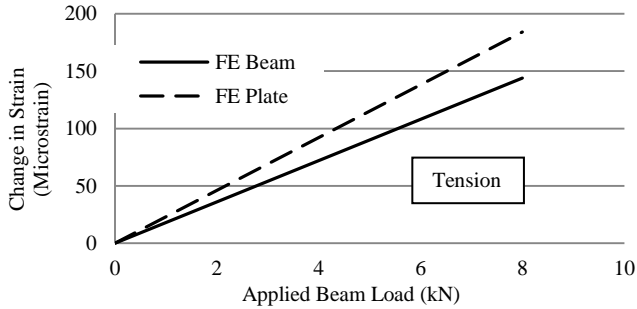


Fig. 9. Phase 3: Predicted Change in Strain vs. Applied Load (FEA)

It was determined the issue with the stress concentration in the central region of the plate caused by the use of a single dowel for fixing, the amplification of the strain signal was low. Hence, an additional FEA was then required to determine the effect fixing the plate to the beam via two dowels at either end of the plate. This was done to attempt to utilise the full cross-sectional area of the wider section of the plate to ensure maximum amplification at the narrow section. This provided a significantly improved strain distribution and hence indicated that it was more effective to have a double dowel system .

VII. PHASE 4: PLATE SENSITIVITY ANALYSIS AND TESTING

A. Testing Procedure

The FEA developed was then used to carry out a sensitivity analysis to determine most efficient and practical plate geometry. The following factors were considered, the dowel offset, the thickness of the plate, the dowel diameter and the width of the tapered area. The dowel offset refers to the distance the plate is offset from the concrete surface and all dowels had the same embedment length of 50mm. The control values for the FEA model were; dowel diameter: 10mm, dowel offset: 10mm, width at centre: 10mm plate thickness: 2mm. The variables were dowel diameter: 5-20mm, dowel offset: 10-100mm, width at centre: 10-85mm plate thickness: 1-10mm, with only one parameter changing at any one time. Six stainless steel plates were fabricated, with welded dowels, to validate the FEA predictions. Table 1 details the variables in this phase of testing. As the magnification of strain is related to the difference in the cross-sectional areas, Plate 5 was fabricated with a tapered thickness as shown in Fig. 10.

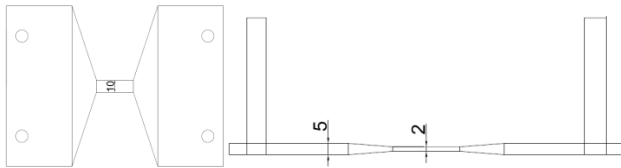
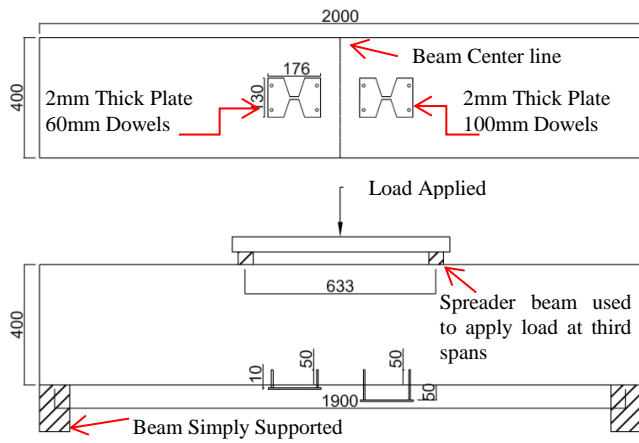


Fig. 10. Phase 4: Geometry of Plate 5, all dimensions in mm

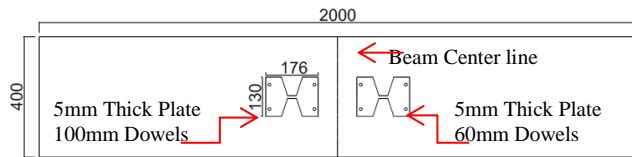
TABLE I
PHASE 4: PLATE GEOMETRY

Test no.	1		2		3	
Plate no.	1	2	3	4	5	6
Thickness (mm)	2	2	5	5	5 to 2*	8
Dowel Length (mm)	60	100	60	100	100	100
Plate offset from concrete (mm)	10	50	10	50	50	50

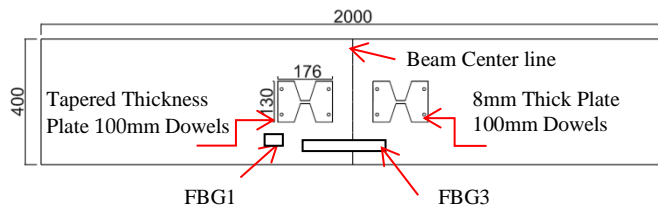
*tapered thickness in order to further reduce ratio of cross sectional area,



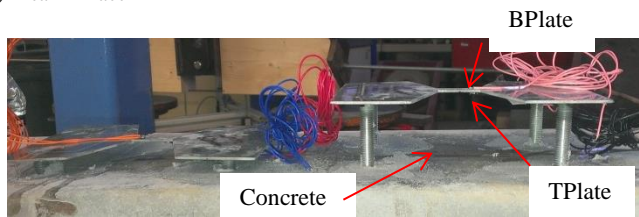
(a) Beam 1 Face 1



(b) Beam 1 Face 2



(c) Beam 2 Face 1



(d) Sensor Locations

Fig. 11. Phase 4: Test configurations.

The plates were fixed in a similar manner as described in Phase 3. The dowels, which were welded to the plates, were embedded into 2m long by 400mm deep by 400mm wide reinforced concrete beams. The configuration of each of the sensors and plates is detailed in Fig. 11. Two separate concrete beams were used and three test loads were carried out.

FBG optical sensors are highly accurate for measuring rapid, dynamic changes and give long-term performance for monitoring concrete bridges. However, for low scanning rates and short-term testing where environmental conditions are not an issue (as in these laboratory trials) ERS sensors can be more cost effective. ERS1 sensors were attached to both sides of the plates and one ERS2 sensor was attached to the surface of the concrete directly below the plate (see Fig. 11). The offset of the instrumented plates are given in Table 1 and Fig. 11(d) shows the sensor/plate locations. TPlate is the face of the plate between the beam and plate, BPlate is opposite face of the plate.

Tests 1 & 2 were used to determine the effect of the dowel length and the test configuration is shown in Fig. 11(a) & (b). Plates 1 & 2 were fixed to the surface of Beam 1, face 1 and had a uniform thickness of 2mm. Plate 1 had a dowel length of 60mm (offset 10mm from concrete surface) and Plate 2 had a 100mm dowel length (offset 50mm from the concrete surface). The beam was set up as shown in Fig. 12, with face 1 to the underside. For Test 2, Beam 1 was turned through 90° and tested with face 2 now on the underside. Plates 3 & 4 were fixed to the surface of face 2 and had a uniform thickness of 5mm. Test 3 on Beam 2, with face 1 at the underside and was used to measure the effect of plate thickness. This test also used additional sensors to accurately measure the actual change in strain on the concrete surface, namely three ERS2 (A-C), one FBG1 and one FBG3 (Fig. 11(c)). All of the results from tests in Phase 4 were compared to assess the effect of the plate thickness on strain amplification.

For all tests the concrete beams were simply supported under the test rig and loaded at the third spans to enable pure flexure in the central region of the beam, as shown in Fig. 12. Load was applied incrementally using an accurately calibrated 600kN capacity hydraulic actuator. Load was applied in 1kN increments under load control with strain readings recorded at each increment of load. For test 1 and 2 a maximum load of 29kN was applied to the beam with readings recorded at ~1kN intervals. Based on the results of Test 1 and 2, the maximum load for Test 3 was reduced to 12kN, again with strain reading recorded at 1kN intervals.

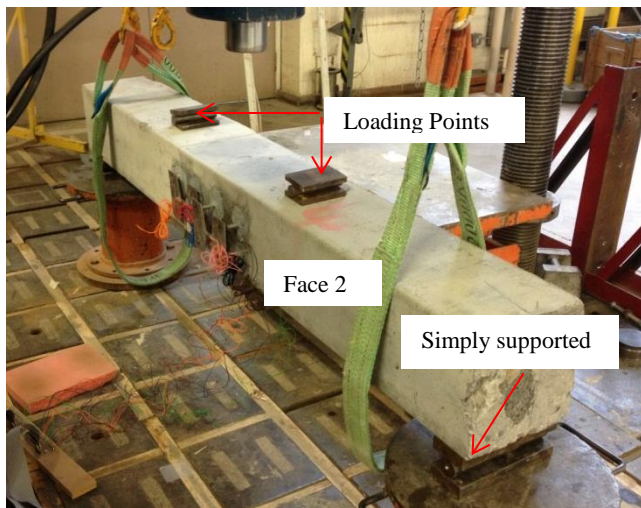
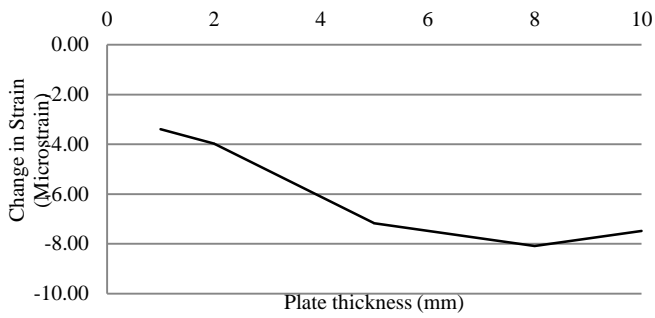


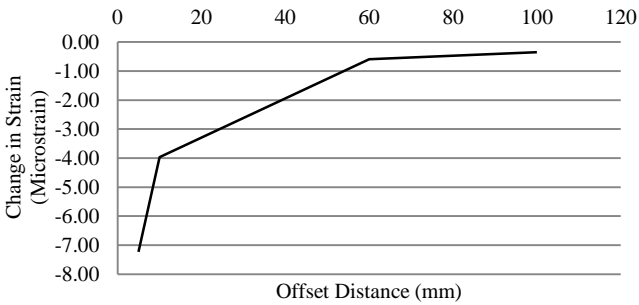
Fig 12. Test Set-up

B. Results and Discussion

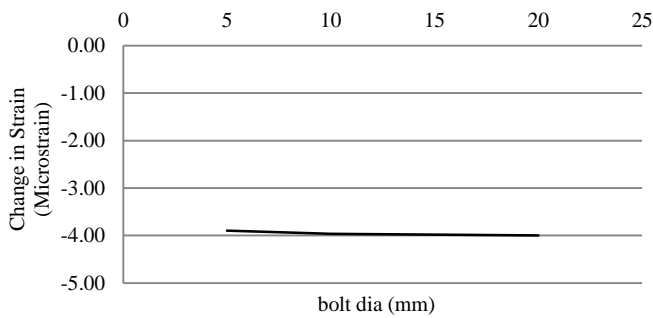
The results from the sensitivity analysis are shown in Fig. 13, the optimum plate thickness was 8mm. However, the 5mm gives similar results and was far most cost effective. The shorter the offset the more amplification occurred and this was tested in the laboratory trials. The bolt diameter had little effect and 10mm was used as a practical and economical solution. The optimum width in the central region was 10mm and this could not be reduced further due to the sensor geometry.



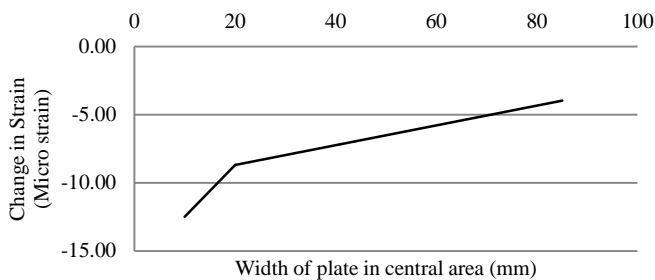
(a) Sensitivity of Strain – overall plate thickness



(b) Sensitivity of Strain - offset distance from the surface of concrete



(c) Sensitivity of Strain - diameter of the fixing dowel.



(d) Sensitivity of Strain - width of the central area.

Fig. 13. Data showing results from FE sensitivity analysis.

1) Phase 4: Test 1 Results

In order to compare the strain amplification in Plates 1 and 2, the change in strain recorded by the BPlate sensors is shown in Fig. 14. Test 1 showed that the shorter dowel length gave a higher amplification of strain and confirmed the predictions from the FEA sensitivity analysis. When a load of 29kN was applied, the measured changes in strain from the BPlate sensors were $-16\mu\epsilon$ and $-8\mu\epsilon$ in Plate 1 and 2 respectively. However, it was found that by removing the bending strains, a reduced amplification was achieved. Hence by including the bending strain a higher amplification of strain can be achieved provided the sensor system is correctly calibrated. In practice, when using this sensor technology for B-WIM, the calibration will be under a known axle load and gross vehicle weight. This amplified reference strain can then be used to calculate unknown axle loads from the subsequent recorded peak strains. Therefore, if the bending strain is utilised to amplify the strain signal, the system is calibrated using this change in strain for each peak in strain under the crossing axle load. The results, from Phase 4 Test 1, also indicated that the most suitable position for maximum strain amplification was at the BPlate sensor location.

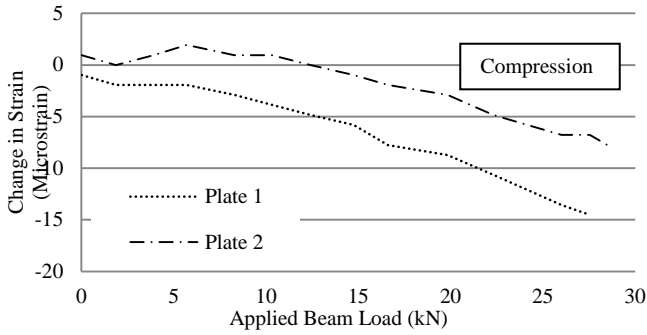


Fig. 14. Phase 4- Test 1: Comparison of BPlate sensors

2) Phase 4 : Test 2 Results

Test 2 confirmed that greater amplification was achieved when the plate was located closer to the surface of the concrete; as indicated by the results in Fig. 15. Test 2 showed that the shorter dowel length gave a higher amplification of strain and confirmed the predictions from the FEA. When a load of 29kN was applied, the measured change in strain from the BPlate sensors on Plates 3 & 4 were $-50\mu\epsilon$ and $-29\mu\epsilon$ respectively. Therefore, the optimum location of the plate was as close as possible to the surface of the concrete structure whilst allowing for curvature of the concrete section under live traffic loading.

The results from Test 1 & 2 were used to determine a suitable thickness of plate between 2mm & 5mm. At an applied load of 29kN, the measured change in strain (from the BPlate sensors) was $-16\mu\epsilon$, $-8\mu\epsilon$, $-50\mu\epsilon$ and $-29\mu\epsilon$ for Plates 1, 2, 3 and 4 respectively (Fig. 16). This indicated that Plate 3 gave the highest amplification of strain as the strain in the concrete surface was similar for all tests at the same applied load. ERS sensors, attached to the concrete surface, were intended to measure the actual change in concrete tensile strain and the results are shown in Fig. 17. It appears that the ERS gauges appear to have de-bonded when cracking occurred at an applied load of 5kN. Minor cracks were visible in the concrete and these ERS sensors were susceptible to debonding when attached to the concrete surface. Therefore it was not possible to determine the actual strain amplification factor as the ERS sensor had failed. These tests indicated that the fixing mechanism for the ERS sensors, under these testing conditions, was not adequate for measuring the change in strains at higher load levels.

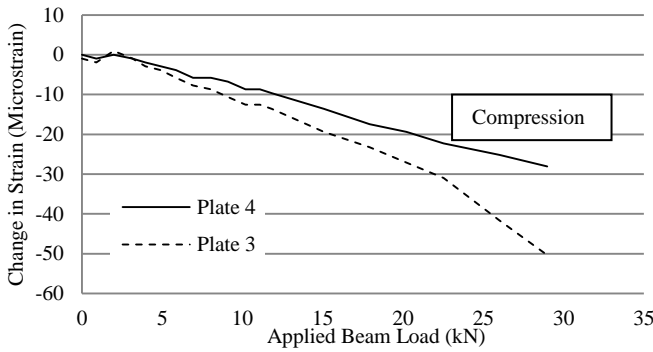


Fig. 15. Phase 4 -Test 2: Comparison of BPlate sensors.

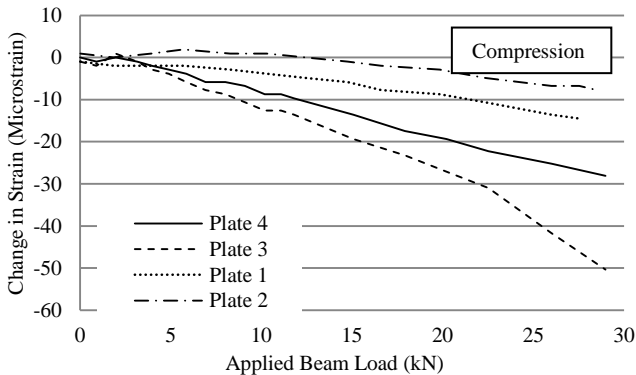


Fig. 16. Phase 4 - Tests 1 & 2: Comparison of Plates 1 to 4

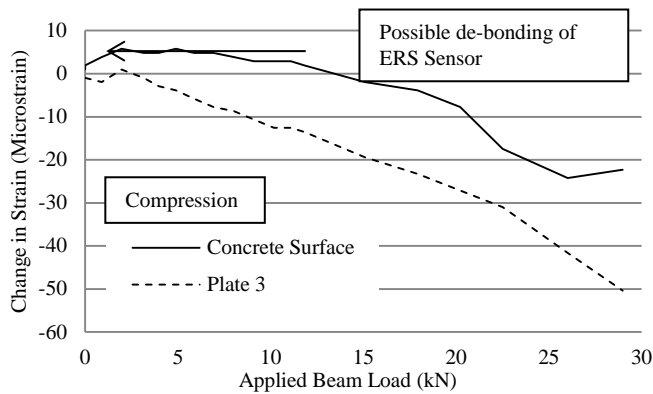


Fig. 17. Phase 4: Comparison of Plate 3 strains and concrete strains

3) Phase 4: Test 3 Results

Tests 1 & 2 showed that the most suitable fixing for the plate was at a minimum offset. However, the plates in this test had been fabricated and embedded in the concrete prior to completing Tests 1 & 2 and the offset for Plates 4 & 5 was 50mm. Test 3 was carried out to provide a further comparison of the effect of plate thickness by testing plates 5 & 6. A maximum load of 12kN was applied as this was below the concrete tensile cracking load in beam 2. The change in strain at the concrete surface was measured using FBG and ERS sensors (as shown in Fig. 11(c)). Due to the close proximity of FBG1 and ERS2C, it was expected that a similar change in strain would be measured from both sensors. At an applied load of 12kN, ERS2C and FBG1 measured a change in strain of $40\mu\epsilon$ and $39\mu\epsilon$ respectively (Fig. 18) and there was no evidence of debonding in these sensors. Fig. 18 also shows that ERS2A and ERS2B recorded lower strain than FBG2, at the maximum applied load. FBG3, ERS2 (A & B) measured a change in strain of $42\mu\epsilon$, $34\mu\epsilon$ and $32\mu\epsilon$ respectively. ERS2 (A & B) were fixed to the concrete surface underneath the plates and may have been affected by the fixing points of the dowels. The strain measured in the concrete was reasonably accurate and was used to determine the strain amplification factor from the Bplates sensors. Fig. 19 shows the change in strain for all plates with an offset of 50mm to determine the most effective plate thickness for strain amplification. This test confirmed that the optimum thickness for the plate was 5mm. However, the strain readings show that the plate did not amplify the induced strain at the concrete surface but the tapered plate (in plan) does give higher strain values than a straight plate. At an applied load of 12kN, the maximum change in strain recorded by the BPlate sensor was $10\mu\epsilon$ compared with a concrete surface strain of $42\mu\epsilon$ recorded by FBG3. Further FEA showed that this was due to the fixing method as the dowels may not provide adequate strain transfer and the method of fixing was adjusted for site applications. Fig. 20, shows the adapted plate where the blocks were fixed directly to the concrete surface giving an offset of 10mm and Plate 3 geometry was used to give maximum strain.

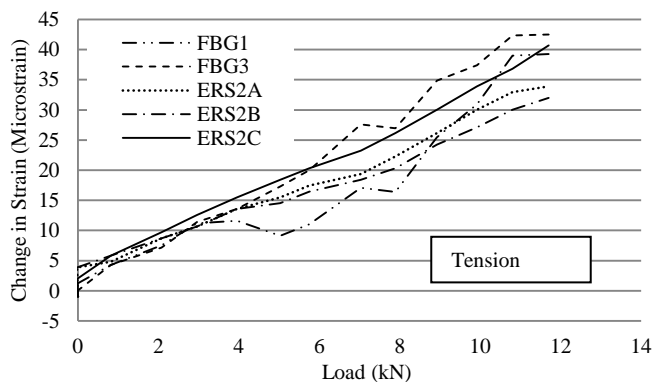


Fig. 18. Phase 4: Test 3 Performance comparison of sensors measuring change in concrete strain

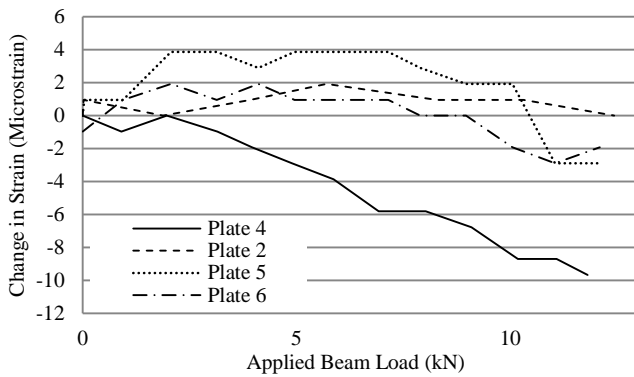


Fig. 19. Phase 4: Comparison of BPlate sensors from all tests.

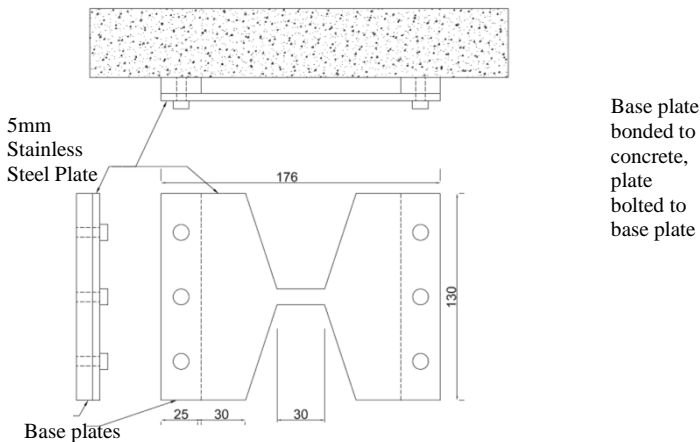


Fig. 20. Geometry of final proposed plate.

VIII. INSTALLATION AT BRIDGE STRUCTURE

The optimum plate geometry as determined from Phase 4 was trialled on a real bridge site to test the amplification in strain under live traffic loading. The plate was instrumented with an FBG1 sensor and fixed to the underside of the longitudinal concrete beam. Another FBG1 sensor was fixed directly to the concrete surface of the beam. Both sensors were orientated to measure a change in longitudinal strain in the beam as shown in Fig. 21. The base plates were fixed to the concrete beam using a two part filled epoxy adhesive system, both surfaces were cleaned and prepared to remove any grease or loose dirt. The surface of the base plate was roughened to ensure a strong grip was obtained.

The data shown in Fig. 22 confirms that strain amplification was successful under live axle loading. The sensor measuring strain directly from the surface of the beam recorded a change in strain of $11\mu\epsilon$ and the sensor fixed to the plate measured a change in strain of $20\mu\epsilon$ under the same load. The vehicle in this example was a typical 5 axle heavy good vehicle and the results show an amplification factor of ~ 2 . This means that lower axle loads can be measured with increased accuracy than by measuring the direct strain in the concrete surface.

IX. DISCUSSION AND CONCLUSIONS

The overall aim of this research was to find a sensor suitable for use in field trials of a new B-WIM system. A series of sequential test programmes has been carried out to determine the most suitable type of sensor and then develop a suite of sensors for B-WIM applications. ERS, VW and FBG-based fibre optic sensors and different fixing techniques were compared.

Phase 1 was a performance comparison of the sensor types and showed that the FBG based sensors to be the most suitable sensor to provide accurate readings at a high scanning rate. The reasons for this are principally associated with capability of existing interrogation units, which can provide scanning rates up to 2000Hz. The maximum scanning rate for the VW sensors was 0.2Hz which made them unsuitable for B-WIM application. In a field environment it is important that the system can be easily and accurately installed, hence difficulties associated with the method of attachment of the ERS sensors regarded them as unsuitable for the proposed system. By contrast, the FBG sensors were quick and easy to install and demonstrated the ability to measure change in strain at high scanning rates. This gave confidence in the sensor type and subsequently the FBG1 sensor type was determined as the most suitable due to its size and ease of fixing. ERS sensors were found to provide results which corresponded well with those obtained from the FBG sensors. As the limiting factor of the ERS sensors was the scanning rate they were suitable for testing fixing methods and strain amplification at low scanning rates. Phase 2 testing aided in the

development of a modified plate which could be used as a means of fixing the sensors to the deck soffit and amplifying the strain readings. The FEA indicated that the geometry of the plate resulted in a stress concentration in small regions of the plate which reduced the strain amplification at the sensor location.



Fig. 21. Arrangement of sensor installed for site trial.

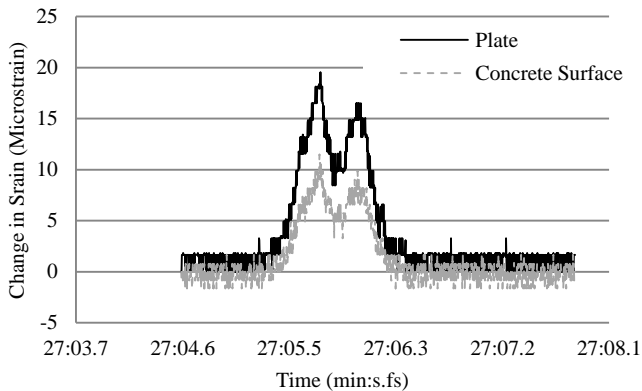


Fig. 22. Strain amplification obtained in field trial

The actual amplification was truly quantified in phase 3 testing; although some amplification was achieved it did not correspond to the amplification anticipated from the theory used to design the plate. The results whilst an improvement from the previous Phase 2 tests did not correlate with the predicted amplification. It was evident from the predicted strain distribution of a further FEA that, the full geometry of the plate was not utilised. The FEA sensitivity analysis worked well to provide an indication to a suitable fixing plate the results from this were then corroborated in the laboratory trials. Test 1 & 2 of Phase four was carried out using only ERS sensors, in some instances it was found that when ERS sensors were fixed directly to the concrete surface the glue initially holding the sensor in place was no longer bonded correctly after minor concrete cracking had occurred. However even in the final Phase of testing an issue with strain transfer to the plate still existed, this loss of strain transfer is thought to be due to the use of dowels as a fixing mechanism.

The final plate design was installed at the bridge site with an adjusted fixing method to provide improved strain transfer between the concrete element and the instrumented plate. The results from live traffic loading at the bridge structure in Fig. 21 show successful strain amplification was achieved. The figure shows the strain was almost doubled; hence the sensor is sensitive to a 0.5 microstrain change making it capable of detecting light axle loads. One issue for further investigation is the possibility of further strain amplification and hence increased sensitivity to lower changed in strain.

In summary, the work carried out in four sequential test series has shown the value of the FBG-based sensors and formed the basis for the design of a fixing plate for the sensors which has been proved to provide strain amplification for monitoring both tensile and compressive strains for applications of this type. On-going research is aimed at evaluating and optimizing the plate design and the overall sensor system.

REFERENCES

- [1] P. Burnos, "Auto-calibration and temperature correction of WIM systems," *ICWIM 5, Proc. Int. Conf.*, pp. 300–307, 2013.
- [2] F. Moses, "No Title," *ASCE Transp. Eng. J.*, vol. 105, pp. 233–249, 1979.
- [3] B. Jacob, E. O'Brien, and S. Jehaes, "Weigh-in-Motion of Road Vehicles: Final Report of the COST 323 Action," Paris, 1999.
- [4] B. Jacob, "Weigh-in-Motion of Axles and Vehicles for Europe (WAVE), General Report," Paris, 2002.
- [5] E. OBrien, M. Quilligan, and R. Karoumi, "Calculating an influence line from direct measurements," *Proc.*, no. March, pp. 31–34, 2006.
- [6] J. Kalin, A. Žnidarič, I. Lavrič, and B. Sc, "PRACTICAL IMPLEMENTATION OF NOTHING-ON-THE- ROAD BRIDGE WEIGH-IN-MOTION SYSTEM," in *International Symposium on Heavy Vehicle Weights and Dimensions*, 2006.
- [7] T. Deesomsuk and T. Pinkaew, "Effectiveness of Vehicle Weight Estimation from Bridge Weigh-in-Motion," *Adv. Civ. Eng.*, vol. 2009, pp. 1–13, 2009.
- [8] K. T. V. Grattan and T. Sun, "Fiber optic sensor technology: an overview," *Sensors and Actuators*, vol. 82, pp. 40–61, 2000.
- [9] Y. M. Gebremichael, W. Li, B. T. Meggitt, W. J. O. Boyle, K. T. V. Grattan, B. McKinley, L. F. Boswell, K. a. Aarnes, S. E. Aasen, B. Tynes, Y. Fonjallaz, and T. Triantafyllou, "A field deployable, multiplexed Bragg grating sensor system used in an extensive highway bridge monitoring evaluation tests," *IEEE Sens. J.*, vol. 5, no. 3, pp. 510–519, Jun. 2005.
- [10] J. Casas and P. Cruz, "Fiber optic sensors for bridge monitoring," *J. Bridg. Eng.*, no. December, pp. 362–373, 2003.
- [11] E. Rivera, D. J. Thomson, and D. Polyzois, "Structural Health Monitoring of Composite Poles Using Fiber Optic Sensors," in *IEEE Canadian Conference On Electrical & Computer Engineering*, 2002.
- [12] D. Inaudi, "Overview of 40 bridge structural health monitoring projects," *Int. Bridg. Conf. IBC*, 2010.
- [13] R. M. Measures, *Structural Monitoring with Fiber Optic Technology*. Academic Press, 2001.
- [14] S. K. T. Grattan, P. a. M. Basheer, S. E. Taylor, T. Sun, and K. T. V. Grattan, "In-situ cross calibration of in-fibre Bragg Grating and Electrical Resistance Strain Sensors for Structural Monitoring using an Extensometer," *IEEE Sens. J.*, vol. 9, no. 11, pp. 1355–1360, 2009.
- [15] S. K. T. Grattan, S. E. Taylor, T. Sun, P. a. M. Basheer, and K. T. V. Grattan, "Monitoring of Corrosion in Structural Reinforcing Bars: Performance Comparison Using In Situ Fiber-Optic and Electric Wire Strain Gauge Systems," *IEEE Sens. J.*, vol. 9, no. 11, 2009.
- [16] M. LYDON, S. TAYLOR, and C. DOHERTY, "Structural Monitoring of the Restoration of Titanic's Dry Dock," *212.8.206.21*, pp. 1–8, 2012.
- [17] K. Hoffmann, "Practical hints for the installation of strain gages," ... *Wheatstone Bridg. Circuit, Doc. HBM*, 1979.
- [18] J. F. Doyle, *Modern Experimental Stress Analysis: Completing the Solution of Partially Specified Problems*. 2004, p. 440.